

Article

Catalytic Synthesis of N-Heterocycles via Direct C(sp³)-H Amination using an Air-stable Iron(III) Species with a Redox-Active Ligand

Bidraha Bagh, Daniël L. J. Broere, Vivek Sinha, Petrus F. Kuijpers, Nicolaas van Leest, Bas de Bruin, Serhiy Demeshko, Maxime A. Siegler, and Jarl Ivar van der Vlugt

J. Am. Chem. Soc., **Just Accepted Manuscript** • DOI: 10.1021/jacs.7b00270 • Publication Date (Web): 15 Mar 2017

Downloaded from <http://pubs.acs.org> on March 16, 2017

Just Accepted

“Just Accepted” manuscripts have been peer-reviewed and accepted for publication. They are posted online prior to technical editing, formatting for publication and author proofing. The American Chemical Society provides “Just Accepted” as a free service to the research community to expedite the dissemination of scientific material as soon as possible after acceptance. “Just Accepted” manuscripts appear in full in PDF format accompanied by an HTML abstract. “Just Accepted” manuscripts have been fully peer reviewed, but should not be considered the official version of record. They are accessible to all readers and citable by the Digital Object Identifier (DOI®). “Just Accepted” is an optional service offered to authors. Therefore, the “Just Accepted” Web site may not include all articles that will be published in the journal. After a manuscript is technically edited and formatted, it will be removed from the “Just Accepted” Web site and published as an ASAP article. Note that technical editing may introduce minor changes to the manuscript text and/or graphics which could affect content, and all legal disclaimers and ethical guidelines that apply to the journal pertain. ACS cannot be held responsible for errors or consequences arising from the use of information contained in these “Just Accepted” manuscripts.

Catalytic Synthesis of N-Heterocycles via Direct C(sp³)-H Amination using an Air-stable Iron(III) Species with a Redox-Active Ligand

Bidraha Bagh,[†] Daniël L. J. Broere,[†] Vivek Sinha,[†] Petrus F. Kuijpers,[†] Nicolaas P. van Leest,[†] Bas de Bruin,^{*,†} Serhiy Demeshko,[#] Maxime A. Siegler,[‡] Jarl Ivar van der Vlugt^{*,†}

[†]Homogeneous, Bioinspired and Supramolecular Catalysis, van 't Hoff Institute for Molecular Sciences, University of Amsterdam, Science Park 904, 1098 XH, Amsterdam, the Netherlands.

[#]Institut für Anorganische Chemie, Georg-August-Universität Göttingen, Tammannstraße 4, 37077 Göttingen, Germany.

[‡]Small Molecule X-ray Crystallography, Department of Chemistry, John Hopkins University, Baltimore MD 21218, USA.

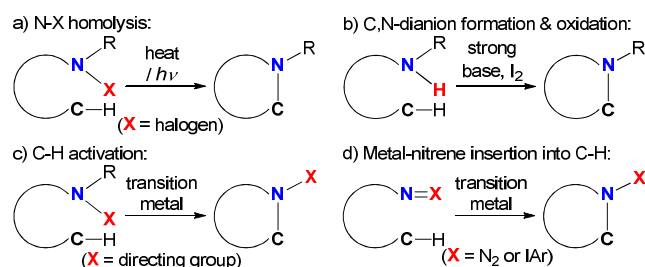
ABSTRACT: Coordination of FeCl₃ to the redox-active pyridine-aminophenol ligand NNO^{H2} in the presence of base and under aerobic conditions generates FeCl₂(NNO^{15Q}) (**1**), featuring high spin Fe^{III} and an NNO^{15Q} radical ligand. The complex has an overall *S* = 2 spin state, as deduced from experimental and computational data. The ligand-centered radical couples anti-ferromagnetically with the Fe center. Readily available, well-defined and air-stable **1** catalyzes the challenging intramolecular direct C(sp³)-H amination of unactivated organic azides to generate a range of saturated N-heterocycles with the highest TON (1 mol% **1**, 12 h, TON = 62; 0.1 mol% **1**, 7 d, TON = 620) reported to date. The catalyst is easily recycled without noticeable loss of catalytic activity. A detailed kinetic study for C(sp³)-H amination of 1-azido-4-phenylbutane (**S**₁) revealed zero order in azide substrate and first order in both catalyst and Boc₂O. A cationic iron complex, generated from the neutral precatalyst upon reaction with Boc₂O, is proposed as the catalytically active species.

INTRODUCTION

The development of efficient methods for the formation of carbon–nitrogen (C–N) bonds is one of the most crucial tasks in chemical synthesis. The installment of C–N bonds by direct functionalization of C(sp³)-H bonds is a powerful and atom-efficient transformation for chemical synthesis. Although the direct installation of nitrogen into a C(sp³)-H bond is extremely challenging due to the thermodynamic and kinetic stability of the C(sp³)-H bond, intra- and intermolecular C(sp³)-H amination has seen much progress in the last decade.¹ Particularly, intramolecular C(sp³)-H amination as an atom-economical strategy has found extensive applications for the construction of varieties of important N-heterocycles.² Four main strategies have been developed for the construction of C(sp³)-H bonds by direct, intramolecular amination of either activated or unactivated C(sp³)-H bonds. A crucial advance in intramolecular C(sp³)-H amination can be traced back to the Hofmann-Löffler-Freytag (HLF) reaction, developed in the early 1880s with the initial discovery by Hofmann.³ N-halogenated amines are utilized as starting materials in HLF reactions and the generally accepted mechanism involves a free radical pathway (Scheme 1a).⁴ Another effective method involves the oxidation of C,N-dianions generated by successive deprotonation of an N-H and a C-H bond, followed by oxidative

coupling under strongly basic conditions (Scheme 1b).⁵ Recently, transition metal catalyzed (predominantly palladium) amination has emerged for the activation of aliphatic C-H bonds, which typically requires an electron-withdrawing directing group (Scheme 1c).⁶ Lastly, nitrene (in situ generated) insertion into a C(sp³)-H bond is an efficient and perhaps the best studied approach for C(sp³)-N bond formation (Scheme 1d). Nitrenes can either be generated from amines by utilizing a combination of PhI(OAc)₂ and MgO or from activated, non-aliphatic organic azides (e.g. sulfonyl azide, aryl azide) or iminoindanes in the presence of transition metal catalysts.⁷

Scheme 1. Intramolecular C(sp³)-H amination strategies for the formation of N-heterocycles.



Unfortunately, most of the existing C–H amination strategies involve directing groups, pre-oxidation of substrates, or external chemical oxidants, leading to poor atom economy and waste generation. In contrast, in situ generation of a metal-bound nitrene species from readily available aliphatic organoazides, releasing only molecular nitrogen as side product, followed by selective insertion into a C(sp³)–H bond would constitute an efficient approach for catalytic C–H amination. Synthesis of N-heterocycles via direct C(sp³)–H amination using aliphatic azide substrates is an appealing strategy, given that N-heterocycles are prevailing building blocks in natural products, pharmaceuticals and functional materials (Figure 1a).⁸ Recently, two reports appeared on air-sensitive Fe^{II}-catalyzed direct C(sp³)–H amination of linear azides to give saturated Boc-protected N-heterocycles, proposedly proceeding via an Fe^{III}-nitrene radical intermediate (Figure 1b).^{9,10} Apart from these systems featuring a redox-active metal center ('metalloradical' approach),¹¹ our group recently demonstrated the catalytic Pd^{II}-mediated C(sp³)–H amination of aliphatic azide to pyrrolidine, albeit with very modest turnover. This system operates via single electron transfer from an aminophenol-derived redox-active ligand to the substrate to generate a Pd-bound nitrene-substrate radical and the one-electron oxidized iminosemiquinonato (ISQ) ligand radical (Figure 1b).¹² Herein we discuss the synthesis and detailed characterization of a bench-stable iron(III) complex with a redox-active NNO ligand. This air-stable iron species is an effective and recyclable catalyst for direct C(sp³)–H amination of aliphatic azides to N-heterocycles with much improved TON's compared to the existing catalysts.

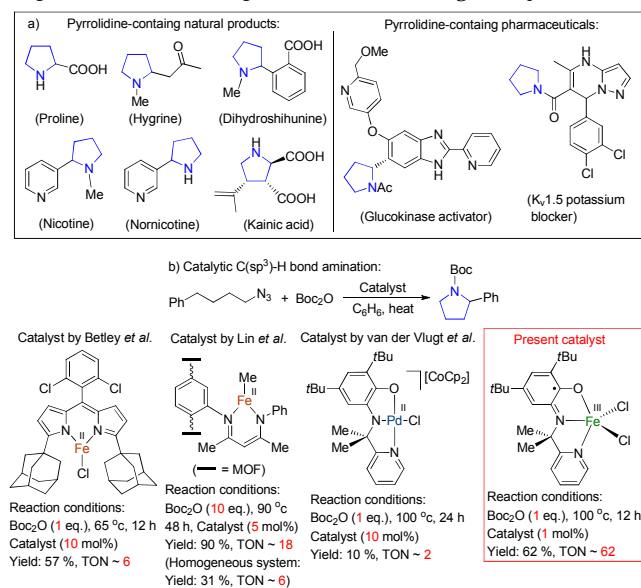


Figure 1. (a) Pyrrolidine-containing natural products and pharmaceuticals and (b) catalysts for direct C(sp³)–H amination of 1-azido-4-phenylbutane as benchmark substrate.

RESULTS AND DISCUSSION

The ligand NNO^{H₂} is readily accessible following a literature procedure.^{12a} Coordination of the neutral ligand NNO^{H₂} to FeCl₃ in MeOH at –80 °C followed by the addi-

tion of NEt₃ in air resulted in the paramagnetic dark green solid **1** in good yield (Scheme 2). UV-vis spectroscopy supports the imino-semiquinonato (ISQ) ligand oxidation state ($\lambda_{\text{max}} = 740 \text{ nm}$, $\epsilon = 8.37 \times 10^3 \text{ M}^{-1} \text{ cm}^{-1}$).^{13–16} Magnetic susceptibility measurements of **1** at 298 K using the Evans' method revealed an effective magnetic moment (μ_{eff}) of 4.86 μ_{B} , thus indicating an $S = 2$ ground state, which is consistent with a high spin Fe^{III}-center (d^5) that is strongly anti-ferromagnetically coupled with a ligand centered NNO^{ISQ} radical. Temperature dependent solid state SQUID measurement and zero-field ⁵⁷Fe Mössbauer spectroscopy confirmed the total $S = 2$ ground state ($\chi_{\text{M}}T = 3.7 \text{ cm}^3 \text{ mol}^{-1} \text{ K}$ or $\mu_{\text{eff}} = 5.44 \mu_{\text{B}}$) and an Fe^{III} oxidation state ($\delta = 0.42 \text{ mm/s}$, $\Delta E_{\text{Q}} = 0.85 \text{ mm/s}$), respectively (Figure 2).¹⁷

Scheme 2. Synthesis of **1**, with representation of three possible oxidation states of NNO.

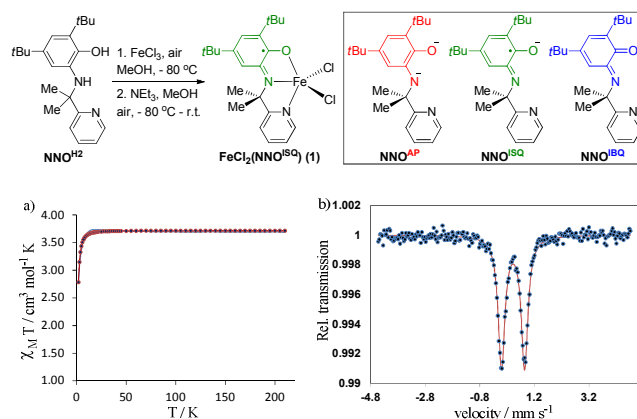


Figure 2. Solid state characterization of **1** by (a) variable temperature SQUID magnetometry and (b) zero-field ⁵⁷Fe Mössbauer spectroscopy at 80 K.

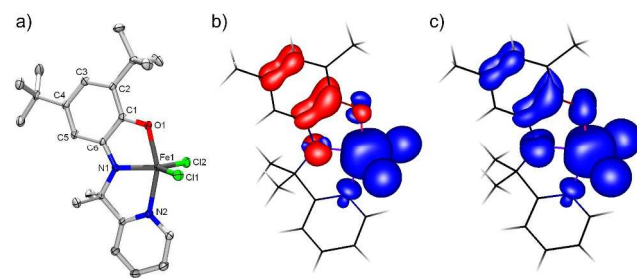


Figure 3. (a) Displacement ellipsoid plot (50% probability level) of **1**; hydrogen atoms and lattice solvent molecules omitted for clarity. Selected bond lengths (Å) and angles (°): Fe(1)–Cl(1) 2.2512(4); Fe(1)–Cl(2) 2.2366(4); Fe(1)–O(1) 1.9572(10); Fe(1)–N(1) 2.0136(12); Fe(1)–N(2) 2.1024(11); C(1)–O(1) 1.2809(17); C(6)–N(1) 1.3390(17); C(1)–C(6) 1.4634(18); O(1)–Fe(1)–N(1) 78.99(4); N(1)–Fe(1)–N(2) 77.56(4); O(1)–Fe(1)–N(2) 156.18(4); Cl(1)–Fe(1)–Cl(2) 117.32(2). DFT (Mo6, def2-TZVP) calculated spin density plot of (b) ground state of **1** ($S = 2$) (c) high spin state of **1** ($S = 3$).

The formulation of **1** as Fe^{III}Cl₂(NNO^{ISQ}) was further confirmed by single crystal X-ray structure determination (Figure 3a). The geometry around iron (τ of 0.52) is intermediate between trigonal bipyramidal and square pyramidal. The iron-ligand bond lengths (Fe–O 1.9572(10);

Fe-N 2.0136(12) Å) as well as ligand-based interatomic distances (O1-C1 1.2809(17); N1-C6 1.3390(17) Å) are characteristic for the ISQ ligand oxidation state.^{14,18-20} A Metrical Oxidation State (MOS) value of $-0.69 (\pm 0.04)$ ¹⁹ was determined for the NNO^{ISQ} ligand of **1**. DFT calculations (b3-lyp, def2-TZVP) show a broken-symmetry $S = 2$ spin state ($\langle S^2 \rangle = 6.8$) as the ground state (see SI). The energy difference between the broken-symmetry $S = 2$ ground state (Figure 3b) and the high-spin $S = 3$ excited state (Figure 3c) is calculated to be $+5.3 \text{ kcal mol}^{-1}$ by DFT. The spin-density plot for $S = 2$ (Figure 3b) clearly illustrates the observed anti-ferromagnetic coupling between the NNO radical fragment and the Fe center via the coordinated N and O atoms. A Löwdin population analysis²² (see SI) shows that the Fe center has a total spin equivalent to 4 unpaired electrons.

Cyclic voltammetry of **1** in CH₂Cl₂ solution revealed quasi-reversible one-electron oxidation and reduction events at $+0.51 \text{ V}$ and -0.74 V vs. Fc/Fc⁺, respectively (Figure 4a). Chemical oxidation of **1** using silver salts likely afforded Cl⁻ abstraction but no clean species was obtained. Chemical reduction of **1** using CoCp₂ led to formation of homoleptic Fe^{II}(NNO^{ISQ})₂ (**2**). The latter species does not reform Fe^{III}(NNO^{ISQ}) upon re-oxidation. The homoleptic complex **2** was characterized by single crystal X-ray structure determination (Figure 4b and SI). Two crystallographically independent molecules of **2** were found in the asymmetric unit ($P2_1/n$). The geometry around each Fe-metal center is distorted octahedral, with meridionally coordinated NNO ligands. The iron-ligand bond lengths, angles and interatomic distances within the NNO moieties are very similar for both molecules and suggestive of the ISQ ligand oxidation state.^{14,18-20} The iron-ligand bond lengths in complex **2** (average bond distances: Fe-O 1.928 Å, Fe-N_{imino} 1.884 Å, Fe-N_{pyridyl} 1.963 Å) are slightly shorter than in heteroleptic complex **1** (Fe-O 1.957 Å, Fe-N_{imino} 2.014 Å, Fe-N_{pyridyl} 2.102 Å). On the contrary, the ligand-based interatomic distances in **2** (average bond distances: C-O 1.320 Å, C-N_{imino} 1.368 Å) are slightly longer than those in complex **1** (C-O 1.281 Å, C-N_{imino} 1.339 Å). Chemical oxidation of **2** with AgBF₄ resulted in the formation of [Fe^{III}(NNO^{ISQ})₂]BF₄ (**3a**), which was structurally characterized (see SI for details). The chloride derivative of this homoleptic Fe^{III}-system, [Fe^{III}(NNO^{ISQ})₂]Cl (**3b**), was accessible directly by heating a mixture of FeCl₃ and NNO^{H2} (2 molar equiv.) at reflux in the presence of NEt₃ under aerobic conditions.

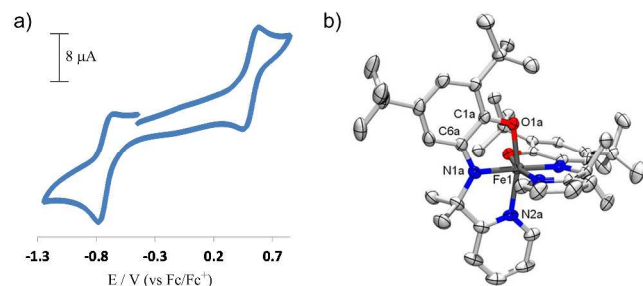


Figure 4. (a) Cyclic voltammogram of **1** in CH₂Cl₂ ($1 \times 10^{-3} \text{ M}$), scan rate 100 mV s^{-1} vs. Fc/Fc⁺ on Pt-disk. (b) Displacement ellipsoid plot (50% probability level) of **2** (one of two independent molecules is shown); hydrogen atoms and lattice solvent molecules omitted for clarity. Selected bond lengths (Å) and angles (°): Fe(1)-O(1A) 1.9267(17); Fe(1)-O(1B) 1.9144(17); Fe(1)-N(1A) 1.890(2); Fe(1)-N(1B) 1.877(2); Fe(1)-N(2A) 1.968(2); Fe(1)-N(2B) 1.957(2); C(1A)-O(1A) 1.314(3); C(1B)-O(1B) 1.324(3); C(6A)-N(1A) 1.367(3); C(6B)-N(1B) 1.375(3); C(1A)-C(6A) 1.433(4); C(1B)-C(6B) 1.439(3); O(1A)-Fe(1)-N(1A) 83.32(8); O(1B)-Fe(1)-N(1B) 84.24(8); N(1A)-Fe(1)-N(2A) 81.62(10); N(1B)-Fe(1)-N(2B) 82.31(9); O(1A)-Fe(1)-N(2A) 164.94(9); O(1B)-Fe(1)-N(2B) 166.04(9); N(1A)-Fe(1)-N(1B) 177.21(9).

We set out to investigate the activity of well-defined air-stable **1** for catalytic C(sp³)-H amination, using 1-azido-4-phenylbutane (**S**₁) as standard substrate and di-*tert*-butyl carbonate (Boc₂O) as in situ protecting group to avoid catalyst deactivation by pyrrolidine coordination (Table 1). Heating an equimolar mixture of both reagents (100 μmol) at 100 °C in benzene for 24 h in the presence of 10 mol% **1** as catalyst in a pressure tube resulted in complete conversion of **S**₁ to the desired Boc-protected pyrrolidine **P**_{1a} (70 %) and Boc-protected amine **P**_{1b} (30%) as side-product (entry 1). Lowering the catalyst loading to 5 mol% led to a slightly different product ratio of 63:37 for **P**_{1a}: **P**_{1b} (entry 2).

Table 1. Performance of 1 in intramolecular C(sp³)-H amination of aliphatic azide **S₁ to **P**_{1a} and **P**_{1b}.**

Entry	1 (mol%)	Boc ₂ O (equiv)	Temp. (°C)	Time (h)	P _{1a} (%)	P _{1b} (%)
1	10	1	100	24	70 (67 ^a)	30
2	5	1	100	24	63 (60 ^a)	37
3 [‡]	5	1	100	24	62	38
4	2	1	100	24	62	38
5	1	1	100	24	62	38

6 [†]	5	5	100	24	63	37
7 [*]	5	10	100	24	65	35

8	5	1	100	2	55	32
9	5	1	100	3	63	37
10 [‡]	5	1	100	3	63	37

12	2	1	100	3	38	17
13	2	1	100	6	62	38
14 [‡]	2	1	100	6	62	38

15	1	1	100	12	62	38
16 [‡]	1	1	100	12	62	38
17 ^{†,‡}	1	1	100	12	52	32

18 [‡]	0.1	1	100	24	11	6
19 [‡]	0.1	1	100	48	23	13

20 [#]	0.1	1	100	168	62	38
21 [#]	10	1	100	24	65	35
22 [#]	5	1	100	24	57	43

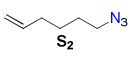
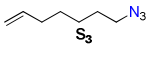
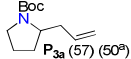
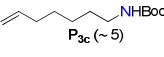
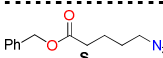
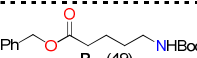
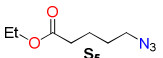
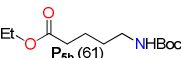
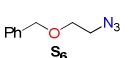
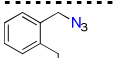
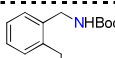
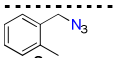
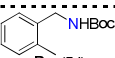
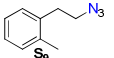
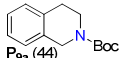
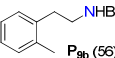
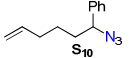
Conditions: [**S**₁] 20 mM, [Boc₂O] 20 mM, **1** (10/5/2/1 mol%), C₆H₆ (5 mL). ¹H NMR yields of **P**_{1a} and **P**_{1b} are reported using 1,3,5-trimethoxybenzene as standard; ^aIsolated yields; ^bRecycled catalyst, ^c[Boc₂O] 50 mM, ^d[Boc₂O] 100 mM. ^eConditions: [**S**₁] 20 mM, [Boc₂O] 20 mM, **1** (0.1 mol%), C₆H₆ (25 mL). ^fConditions: [**S**₁] 20 mM, [Boc₂O] 20 mM, **1** (10 and 5 mol%), toluene (5 mL). Key parameters for each entry are indicated in red.

Catalyst **1** was successfully recovered by precipitation (dark green precipitate) from the crude reaction mixture upon addition of pentane, allowing recycling without any loss of catalytic activity (entry 3). Analysis of the recovered dark green solid by UV-vis spectroscopy (λ_{max} : 740 nm) and mass spectrometry (M^+ : m/z 464.1084) confirmed the structural integrity of complex **1** after catalysis. Based on these observations, we exclude involvement of homoleptic Fe^{II} species **2** as catalytically active species, as this complex cannot regenerate complex **1**. Further reduction of the catalyst loading to 2 or 1 mol% gave full conversion with virtually the same ratio of **P**_{1a}: **P**_{1b} (entry 4 and 5). Using excess Boc₂O at 100 °C did not lead to any change in the product distribution (entries 6 and 7).¹⁰ Monitoring the reaction progress with 5 mol% catalyst loading showed complete conversion already after 3 h (entry 9), also for recovered catalyst (entry 10). Upon reducing the catalyst loading to 2 mol%, we observed approx. 50% conversion of substrate in 3 h (entry 12) and full conversion in 6 h (entry 13). Also in this case, the catalyst was recovered and reused without significant loss of catalytic activity (entry 14). The ratio of **P**_{1a}: **P**_{1b} (~1.6:1) remained constant (entries 12 to 14). Complete conversion of substrate to products was also obtained with 1 mol% catalyst loading already after 12 h (entry 15). Hence, the catalyst can be recovered and reused without significant loss of catalytic activity, using either 5 mol% (entries 3 and 10) or 2 mol% (entry 14) catalyst loading. Heating an equimolar mixture of both reagents (500 μ mol) at 100 °C in benzene (25 mL) for 12 h in the presence of 1 mol% of **1** (5 μ mol) (entry 16) also allowed for facile catalyst recovery by precipitating into pentane. In this case, the reaction did not go to completion in 12 h using the recycled catalyst (entry 17). Besides the two products (**P**_{1a}: **P**_{1b} \approx 1.6:1), roughly 16% unreacted azide (**S**₁) was recovered. Hence, a slight loss of catalytic activity was observed with this recycling at 1 mol% catalyst loading. However, this diminished catalytic activity might be due to partial loss of catalyst during recovery. Thereafter, the catalyst loading was further reduced to 0.1 mol%. We performed the runs with 500 μ mol of **S**₁ and Boc₂O in 25 mL solvent, keeping the effective concentration constant (entries 18 to 20). Lowering the catalyst loading to 0.1 mol% resulted in 17% and 36% conversion of substrate in 24 (entry 18) and 48 h (entry 19), respectively, with a product ratio of ~1.6:1 (**P**_{1a}: **P**_{1b}). The highest turnover number (TON) of 620 was obtained with 0.1 mol% catalyst loading after a week of heat-

ing (entry 20). Changing from benzene to toluene did not have a significant influence on the outcome (entries 21 and 22) and only minor differences in product ratio were observed. A large scale reaction (**S**₁: 500 μ mol, Boc₂O: 500 μ mol, catalyst: 5 mol%) resulted in an isolated yield for **P**_{1a} of 62% (see supporting information). Therefore, catalyst **1** allows significantly higher turnover numbers than previously reported homogeneous systems (maximum TON of ~6)^{9a,10} for the direct intramolecular C(sp³)-H amination of unactivated organic azide.

We explored several additional substrates for the intramolecular C(sp³)-H amination catalyzed by complex **1** (Table 2 and SI). Complete conversion of substrates **S**₂ to **S**₁₀ to the corresponding N-heterocycles and linear amines was observed in 24 h at 100 °C using 5 mol% catalyst loading.

Table 2. Substrate screening with **1 for C-H amination of aliphatic azides to N-heterocycles and amines.**

Substrate	N-heterocycle	Amine
	 P _{2a} (96 ^b)	No amine
	 P _{3a} (57) (50 ^b)  P _{3b} (38)	 P _{3c} (~5)
	 P _{4a} (51)	 P _{4b} (49)
	 P _{5a} (39)	 P _{5b} (61)
	 P _{6a} (92), (90 ^b)	 P _{6b} (8)
	 P _{7a} (53) (48 ^b)	 P _{7b} (47)
	 P _{8a} (46)	 P _{8b} (54)
	 P _{9a} (44)	 P _{9b} (56)
	 P _{10a} (95 ^b)	No amine

Conditions: [**S**₁] 20 mM, [Boc₂O] 20 mM, **1** (5 mol%), C₆H₆ (5 mL), T = 100 °C, 24 h. ¹H NMR ratios are reported in brackets, determined using 1,3,5-trimethoxybenzene as internal standard; ^aIsolated yields.

Utilizing 1-azido-5-hexene (**S**₂) as substrate, allylic C-H amination occurs cleanly to give five-membered N-heterocycle (**P**_{2a}: 96% isolated yield), and no linear amine byproduct was detected. Both homoallylic and allylic C-H amination occur using 1-azido-6-heptene (**S**₃), generating five- (**P**_{3a}: 57%) and six-membered (**P**_{3b}: 38%) N-heterocycles with traces of undesired amine (**P**_{3c}). The

products \mathbf{P}_{3a} and \mathbf{P}_{3b} are obtained by homo-allylic and allylic C–H bond activation, respectively, with a ratio of 1.5:1.0 ($\mathbf{P}_{3a}:\mathbf{P}_{3b}$). This observation can be considered as support for direct nitrene insertion into the $\text{C}(\text{sp}^3)\text{--H}$ bond, generating both an N–H and C–N bond simultaneously. Combined with the formation of a favorable five-membered ring, the somewhat stronger homo-allylic C–H bond is preferentially activated over the weaker allylic C–H bond. A similar observation (but without explanation) was made by Betley *et al.* for the C–H amination of 1-azido-5-methylhexane, with five-membered pyrrolidine (from secondary C–H bond activation) being the major and six-membered piperidine (from weaker tertiary C–H bond activation) the minor product in a ratio of 1.5:1.0.^{9a} Substrates \mathbf{S}_4 and \mathbf{S}_5 , containing secondary C–H bonds adjacent to an electron-withdrawing ester group were transformed to the corresponding pyrrolidines \mathbf{P}_{4a} (51%) and \mathbf{P}_{5a} (39%). Azide substrate with an oxygen atom in the aliphatic chain (\mathbf{S}_5) gave the oxazolidine product \mathbf{P}_{5a} in high yield (90% isolated yield). Apart from monocyclic products, bicyclic N-heterocycles also proved accessible via this approach. Starting from 1-azidomethyl-2-ethylbenzene (\mathbf{S}_7), containing secondary benzylic C–H bonds, or 1-azidomethyl-2-methylbenzene (\mathbf{S}_8) and 1-(2-azidoethyl)-2-methylbenzene (\mathbf{S}_9) with primary C–H bonds, yielded the desired N-heterocycles (\mathbf{P}_{7a} : 53%; \mathbf{P}_{8a} : 46%; \mathbf{P}_{9a} : 44%). The scope of the intramolecular $\text{C}(\text{sp}^3)\text{--H}$ amination catalyzed by complex $\mathbf{1}$ was also extended to include 1-azido-1-phenyl-5-hexene (\mathbf{S}_{10}) as secondary azide, selectively yielding the desired N-heterocycle \mathbf{P}_{10a} (mixture of rotamers and diastereomers) (95% isolated yield). Furthermore, organoazides containing a vinyl functionality (\mathbf{S}_2 , \mathbf{S}_3 and \mathbf{S}_{10}) provide the desired N-heterocycles (\mathbf{P}_{2a} , \mathbf{P}_{3a} , \mathbf{P}_{3b} and \mathbf{P}_{10a}) with very little or no undesired linear amine or aziridine. We could not find a clear correlation between the bond dissociation energy (BDE) of all types of C–H bonds involved and the outcome of the catalytic reactions.²³

To exclude that the observed catalytic C–H amination activity was due to an impurity originating from the FeCl_3 precursor, we tested the FeCl_3 used for the synthesis of complex $\mathbf{1}$ as a catalyst for the conversion of \mathbf{S}_1 . No conversion to N-heterocycle (\mathbf{P}_{1a}) or linear amine (\mathbf{P}_{1b}) was observed with either 5 or 10 mol% catalyst loading in the presence of 1 equiv. of Boc_2O (in benzene or toluene) at 100 °C for 24 h. When using homoleptic Fe^{III} complex $\mathbf{3b}$, $[\text{Fe}^{\text{III}}(\text{NNO}^{\text{ISO}})_2]\text{Cl}$ (5 or 10 mol%), prepared directly from FeCl_3 and NNO^{H_2} , no product formation was detected. Partial poisoning tests using tetramethylthiourea²⁴ (TMTU; ± 0.3 molar equiv. relative to $\mathbf{1}$) and elemental mercury gave identical conversion and product ratio compared to the standard reaction without these additives. On the basis of these results, we rule out the active participation of (ligand stabilized) trace metal impurities present in the FeCl_3 precursor.²⁵ Thereafter we performed kinetic analysis for the intramolecular $\text{C}(\text{sp}^3)\text{--H}$ amination of \mathbf{S}_1 catalyzed by complex $\mathbf{1}$ (see Tables S4–S6 in SI). Monitoring the reaction progress using 2 mol% catalyst loading (entries 1 to 5), we observed in a linear decrease in

$[\mathbf{S}_1]$ with time, suggestive of saturation kinetics or zero order kinetics in \mathbf{S}_1 (rate constant = $3.5 \mu\text{M h}^{-1}$) (Figure 5a). A constant rate of substrate consumption ($17.5 \mu\text{mol h}^{-1}$) was observed (Figure 5b). The rate of substrate consumption ($\mu\text{mol h}^{-1}$) against the concentration of $\mathbf{1}$ (mM), varied between 1 and 7 mol% (entries 6 to 12) showed first order kinetics in $\mathbf{1}$ (Figure 5c). Performing the $\text{C}(\text{sp}^3)\text{--H}$ amination of \mathbf{S}_1 with different concentrations of Boc_2O (20–60 mM; entries 13 to 17) led to a linear increase in the rate of reaction ($\mu\text{mol h}^{-1}$) (Figure 5d), indicating first order kinetics in Boc_2O . An intramolecular kinetic isotope effect (KIE) of 3.4 was obtained using 1-azido-4-deutero-4-(deuterophenyl)-butane as substrate (Scheme 3). This value is identical to the KIE value (3.4) obtained for the $\text{C}(\text{sp}^3)\text{--H}$ amination of 1-azido-4-deutero-4-phenylbutane catalyzed by the Pd-catalyst recently published by our group.^{12a}

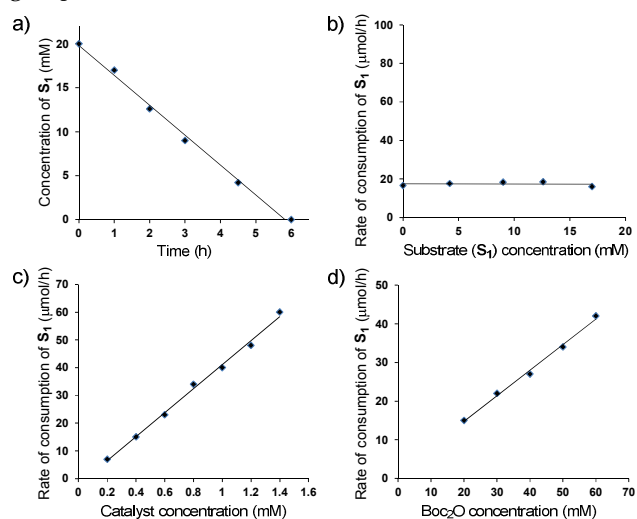
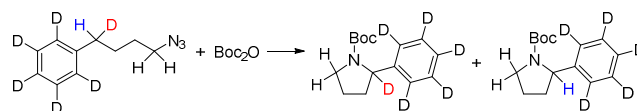


Figure 5. Kinetic analysis for $\text{C}(\text{sp}^3)\text{--H}$ amination of \mathbf{S}_1 in presence of Boc_2O catalyzed by $\mathbf{1}$: a) rate of substrate consumption vs. time, b) rate of substrate consumption vs. substrate concentration, c) rate of substrate consumption vs. concentration of catalyst and d) rate of substrate consumption vs. concentration of Boc_2O .

Scheme 3. Intramolecular kinetic isotope effect in catalytic C–H amination of 1-azido-4-deutero-4-(deuterophenyl)-butane as substrate.

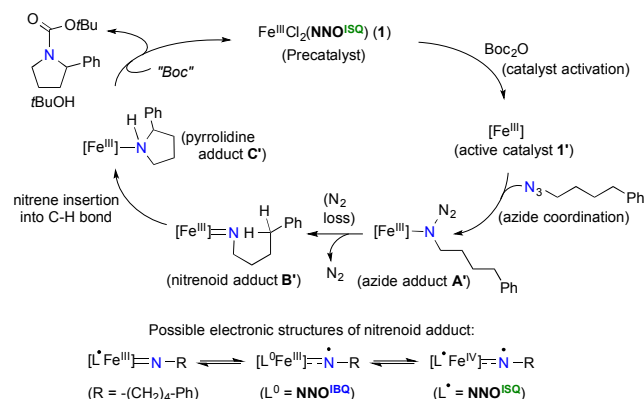


For both Betley's iron-catalyst^{9a} and the palladium-catalyst reported by us,^{12a} $\text{C}(\text{sp}^3)\text{--H}$ amination of unactivated azides was proposed to occur via rate limiting azide activation (release of N_2) and a subsequent radical pathway involving metal- or ligand-based single electron transfer, resulting in the formation of a metal-nitrene radical species. Similar 'nitrene radical' intermediates have recently been spectroscopically characterized for cobalt-porphyrins and other systems.^{26–28} Formation of the saturated N-heterocycle proceeds via either H-atom

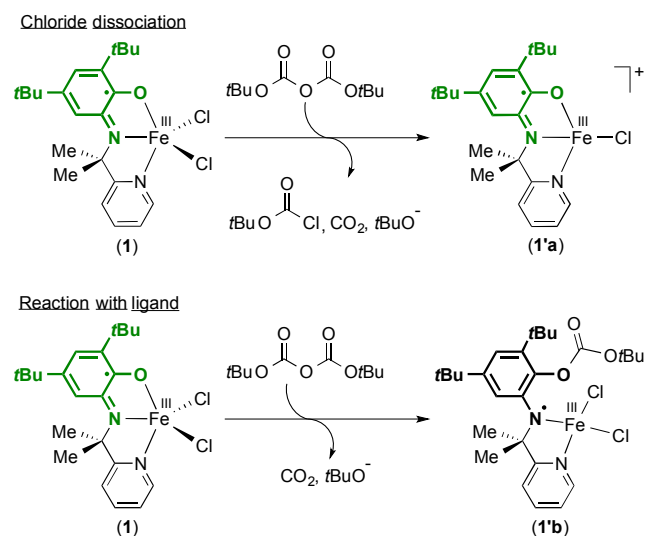
abstraction followed by radical rebound or direct insertion of the nitrene moiety into the benzylic C–H bond then forms a pyrrolidine complex. Finally, reaction with Boc_2O releases the Boc-protected N-heterocycle and regenerates the catalyst (See SI for hypothetical scheme based on **1**).

However, this mechanism, as postulated for other systems, is not in agreement with the observed kinetic data when employing catalyst **1**. The zero order in substrate (S_1) implies that (binding and) activation of the azide substrate is not rate limiting. Reaction of complex **1** with either a stoichiometric amount or excess (5 and 10 times) S_1 in the absence of Boc_2O at r.t. (or high temperature) did not yield intermediate **A** (or **B** or **C**; see SI), and only starting materials were recovered. The first order kinetics in Boc_2O suggests that a reaction with Boc_2O is the rate determining step in the overall $\text{C}(\text{sp}^3)\text{--H}$ amination reaction of S_1 . The active involvement of Boc_2O for catalytic turnover is also suggested by the lack of any product (P_{1a}/P_{1b}) formation from S_1 in the absence of Boc_2O . However, pyrrolidine adduct **C** proved inaccessible by reaction of **1** with (excess) 2-phenylpyrrolidine, speaking against product inhibition in this case. Therefore, we propose an alternative mechanism to explain the kinetic data (Scheme 4). Initial activation of complex **1** by Boc_2O (present in slight excess relative to substrate) at elevated temperature (rate determining step) leads to the activated Fe^{III} catalyst with a higher affinity for the substrate. Two potential ways for Boc_2O to interact with **1** are depicted in Scheme 4: either chloride abstraction or reaction with the phenolate fragment of the redox-active NNO ligand can (pseudo)reversibly generate a cationic Fe^{III} species **1'**.²⁹ Thereafter, facile coordination of the azide-substrate to the metal center gives adduct **A'** and subsequent N_2 elimination generates iron(III)-nitrenoid species **B'**. Either direct nitrene insertion (preferred for (homo)allylic substrates) or H-atom abstraction and radical rebound forms the Fe^{III} (pyrrolidine) adduct **C'**. Finally, reaction with a Boc-containing species (denoted "Boc" in Scheme 4) - either the in situ generated *tert*-butoxycarbonyl chloride or the carbonate derivative of the NNO ligand; see Scheme 5 - releases Boc-protected N-heterocycle (P_{1a}) and *tert*-butanol with regeneration of complex **1**.

Scheme 4. Proposed cationic pathway for the conversion of S_1 to P_{1a} with **1** as catalyst.



Scheme 5. Possible activation steps of catalyst **1** by Boc_2O .



It is reasonable to assume that chloride dissociation from complex **1** generates a four-coordinated cationic complex $[\text{Fe}^{\text{III}}\text{Cl}(\text{NNO}^{\text{ISQ}})]^+$ (**1'a**) or $[\text{Fe}^{\text{III}}\text{Cl}_2(\text{NNO}^{\text{ISQ}}\text{-Boc})]^+$ (**1'b**), which can easily bind an organoazide to generate **A'**. Release of dinitrogen forms an Fe-NR intermediate **B'**, which may exist in various spin states. This eventually forms cationic pyrrolidine-adduct $[\text{Fe}^{\text{III}}\text{Cl}(\text{NNO}^{\text{ISQ}})(2\text{-phenylpyrrolidine})]^+$ (**C'**). Upon reaction of **1** with one equiv. of TIPF_6 as redox-inert halide abstracting agent in the presence of a small excess of S_1 (2.5 equiv.) in THF, a color change from green to blue-green was observed, concomitant with formation of a white precipitate. Mass spectrometric analysis of the filtrate (m/z 614.3342) is in line with formation of the cationic complex $[\text{Fe}(\text{NNO})(2\text{-phenylpyrrolidine})(\text{THF})]^+$.³⁰ This cationic complex was further reacted with Boc_2O (1 equiv.) to cleanly form Boc-protected pyrrolidine P_{1a} , supporting its possible involvement in the proposed catalytic pathway for the C-H amination of S_1 .³¹

Performing the $\text{C}(\text{sp}^3)\text{--H}$ amination of S_1 in presence of excess *t*BuOH, which is generated after coupling of the heterocycle with Boc_2O led to the same $P_{1a}:P_{1b}$ ratio of 63:37 as observed under standard reaction conditions, excluding any role of the alcohol in the formation of the side product. No nitrile or imine by-product was observed under these conditions, which argues against substrate acting as H-atom donor. When carrying out the catalysis at ten-fold higher absolute concentrations of all components (S_1 , Boc_2O and **1**) - to reduce any harmful effects of impurities in the solvent - the $P_{1a}:P_{1b}$ ratio increased significantly ($P_{1a}:P_{1b} = 79:21$; see SI for details). Additional distillation of the solvent or switching from C_6H_6 to C_6D_6 did not affect the product ratio determined by ^1H NMR spectroscopy, which speaks against the solvent acting as a hydrogen source, and suggests the involvement of an unknown impurity at low concentration in the side reactions producing the linear Boc-protected amines.

SUMMARY AND CONCLUSIONS

In summary, straightforward synthesis of complex **1** [$\text{Fe}^{\text{III}}\text{Cl}_2(\text{NNO}^{\text{ISO}})$] gives access to an air-stable and recoverable Fe-catalyst for the efficient direct C(sp³)-H amination of unactivated organic azides to N-heterocycles, providing significantly higher TON's than previously reported with any homogeneous catalyst for this type of transformation. Experimental and computational data suggests that **1** is best described as an Fe^{III} center that is antiferromagnetically coupled to a ligand-centered NNO^{ISO} radical. In addition to the standard azide substrate **S₁**, the scope of C-H amination was extended to eight other primary azides (**S₂** to **S₈**) and a secondary azide (**S₁₀**). Based on the experimental evidence, we propose a mechanism for the C-H amination of organoazides involving catalyst activation by Boc₂O to form an activated cationic species, followed by a cationic azide activation pathway. In addition to the desired N-heterocycles, unwanted linear amines form in most of the cases. However, organoazides containing a vinyl functionality were converted almost exclusively to the preferred N-heterocycles. The origin of the hydrogen required for the formation of linear amine is unclear to date. The exact mechanism of the C-H amination is currently unknown and various redox states as well as spin states are possible for the combination of iron, NNO ligand and a metal-bound nitrene moiety, all of which are potentially redox-active, makes for a complex overall system. However, the observed preference for homo-allylic vs. allylic C-H amination suggests direct nitrene insertion without radical character induced by metal or ligand electron transfer, as the most competent pathway. The catalyst integrity as a heteroleptic species, enabling turnover at relative low catalyst loading as well as catalyst recycling, combined with the versatile coordination chemistry and the potential proclivity to allow various redox spin states are considered key factors that contribute to the overall performance of this system. Detailed computational investigations are ongoing to unravel the mechanism and to determine the metal, ligand and substrate redox states of the key intermediates. Additionally, we are exploring the catalytic activity of complex **1** for intermolecular C-H amination and other types of reactions.

ASSOCIATED CONTENT

Computational data, experimental and analytical details, crystallographic data, spectroscopic details. This material is available free of charge via the Internet at <http://pubs.acs.org>.

AUTHOR INFORMATION

Corresponding Authors

b.debruin@uva.nl; j.i.vandervlugt@uva.nl

Notes

The authors declare no competing financial interest.

ACKNOWLEDGMENT

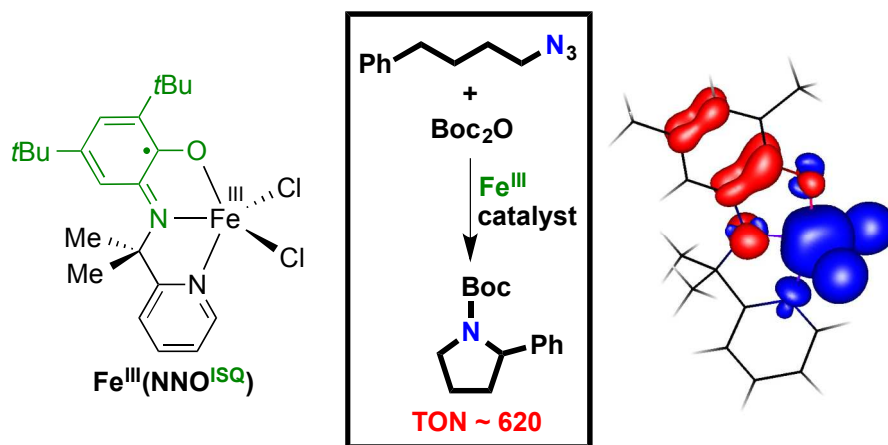
This research was funded by the European Research Council (ERC) through a Starting Grant (Agreement 279097,

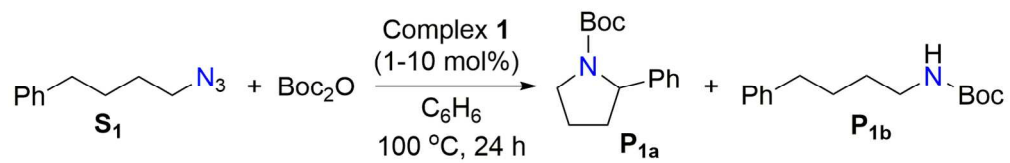
EuReCat) to J.I. van der V. V.S. acknowledges the CSER program of NWO-FOM and Shell for funding and P.F.K. and B. de B. thank NWO (VICI project 016.122.613). We thank Ed Zuidinga for MS analysis, Prof. Joost Reek for interest and support and Prof. Franc Meyer for generous access to the Mössbauer and SQUID equipment in Göttingen.

REFERENCES

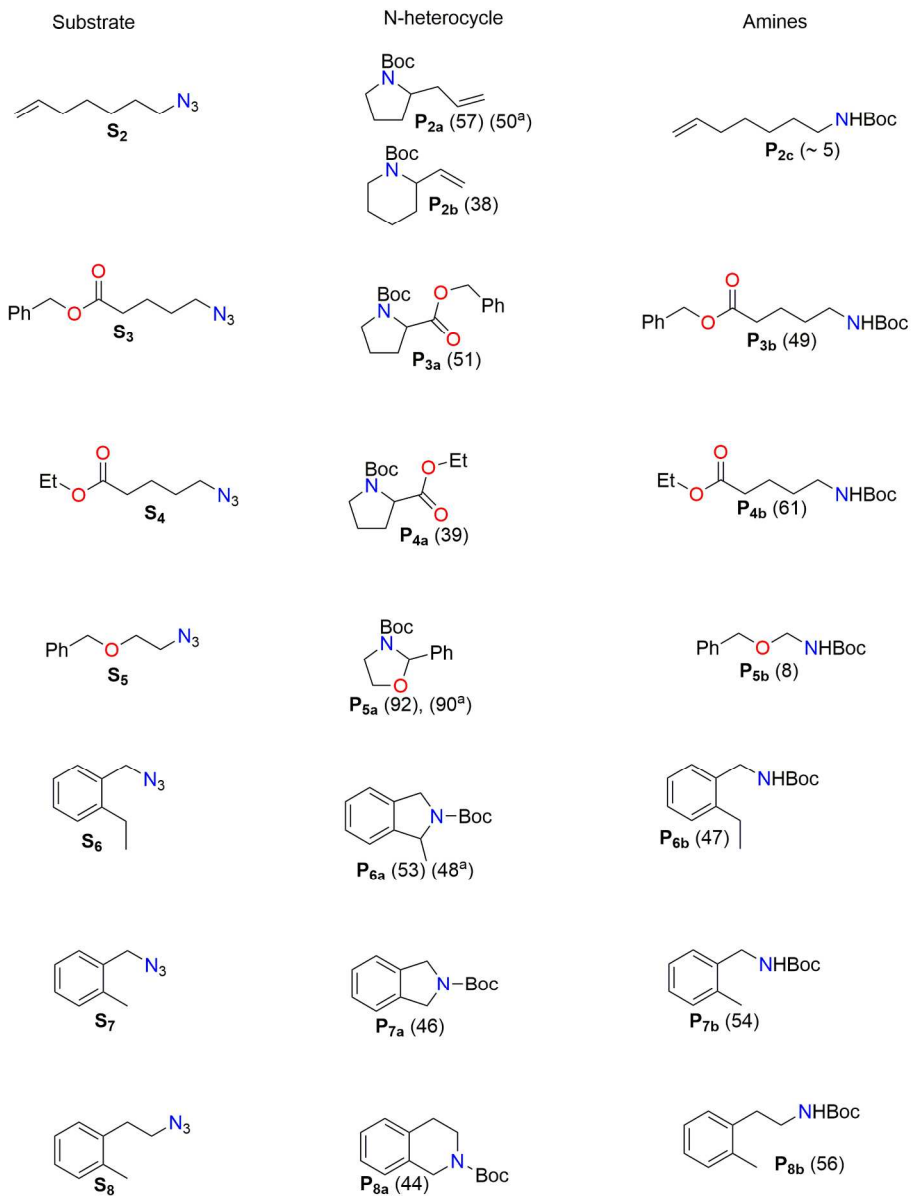
- For selected reviews, see: (a) Collet, F.; Dodd, R.; Dauban, P. *Chem. Commun.* **2009**, 5061-5074. (b) Sun, C.-L.; Li, B.-J.; Shi, Z.-J. *Chem. Rev.* **2011**, *111*, 1293-1314. (c) Ramirez, T.; Zhao, B.; Shi, Y. *Chem. Soc. Rev.* **2012**, *41*, 931-942. (d) Gephart, R. T.; Warren, T. H. *Organometallics* **2012**, *31*, 7728-7752. (e) Intriери, D.; Zardi, P.; Caselli, A.; Gallo, E. *Chem. Commun.* **2014**, 50, 11440-11453. (f) Shin, K.; Kim, H.; Chang, S. *Acc. Chem. Res.* **2015**, *48*, 1040-1052. (g) Guo, X.-X.; Gu, D.-W.; Wu, Z.; Zhang, W. *Chem. Rev.* **2015**, *115*, 1622-1651. (h) Wan, J.-P.; Jing, Y. *Beilstein J. Org. Chem.* **2015**, *11*, 2209-2222.
- Jeffrey, J. L.; Sarpong, R. *Chem. Sci.* **2013**, *4*, 4092-4106.
- (a) Hofmann, A. W. *Ber. Dtsch. Chem. Ges.* **1883**, *16*, 558-560. (b) Hofmann, A. W. *Ber. Dtsch. Chem. Ges.* **1885**, *18*, 5-23.
- (a) Fan, R.; Pu, D.; Wen, F.; Wu, J. *J. Org. Chem.* **2007**, *72*, 8994-8997. (b) Chen, H.; Sanjaya, S.; Wang, Y.-F.; Chiba, S. *Org. Lett.* **2013**, *15*, 212-215. (c) Verma, A.; Patel, S.; Meenakshi; Kumar, A.; Yadav, A.; Kumar, S.; Jana, S.; Sharma, S.; Prasad, C. D.; Kumar, S. *Chem. Commun.* **2015**, 51, 1371-1374. (d) Qin, Q.; Yu, S. *Org. Lett.* **2015**, *17*, 1894-1897. (e) Yamamoto, C.; Takamatsu, K.; Hirano, K.; Miura, M. *J. Org. Chem.* **2016**, *81*, 7675-7684.
- (a) Bisai, A.; West, S. P.; Sarpong, R. *J. Am. Chem. Soc.* **2008**, *130*, 7222-7223. (b) Smith, A. C.; Williams, R. M. *Angew. Chem., Int. Ed.* **2008**, *47*, 1736-1740. (c) West, S. P.; Bisai, A.; Lim, A. D.; Narayan, R. R.; Sarpong, R. *J. Am. Chem. Soc.* **2009**, *131*, 1187-1194. (d) Gruver, J. M.; West, S. P.; Collum, D. B.; Sarpong, R. *J. Am. Chem. Soc.* **2010**, *132*, 13212-13213. (e) Carpenter, R. D.; Verkman, A. S. *Org. Lett.* **2010**, *12*, 1160-1163.
- (a) Neumann, J. J.; Rakshit, S.; Dröge, T.; Glorius, F. *Angew. Chem. Int. Ed.* **2009**, *48*, 6892-6895. (b) Nadre, E. T.; Daugulis, O. *J. Am. Chem. Soc.* **2012**, *134*, 7-10. (c) Yang, M.; Su, B.; Wang, Y.; Chen, K.; Jiang, X.; Zhang, Y.-F.; Zhang, X.-S.; Chen, G.; Cheng, Y.; Cao, Z.; Guo, Q.; Wang, L.; Shi, Z.-J. *Nat. Commun.* **2014**, *5*, 4707-4752. (d) Wu, X.; Yang, K.; Zhao, Y.; Sun, H.; Li, G.; Ge, H. *Nat. Commun.* **2015**, *6*, 6462-6471. (e) Yang, M.-Y.; Jiang, X.-Y.; Shi, Z.-J. *Org. Chem. Front.* **2015**, *2*, 51-54.
- (a) Espino, C. G.; DuBois, J. *Angew. Chem. Int. Ed.* **2001**, *40*, 598-600. (b) Espino, C. G.; When, P. M.; Chow, J.; Du Bois, J. *J. Am. Chem. Soc.* **2001**, *123*, 6935-6936. (c) Liang, J.-L.; Yuan, S.-X.; Huang, J.-S.; Yu, W.-Y.; Che, C.-M. *Angew. Chem. Int. Ed.* **2002**, *41*, 3465-3468. (d) When, P. M.; Du Bois, J. *J. Am. Chem. Soc.* **2002**, *124*, 12950-12951. (e) Hinman, A.; Du Bois, J. *J. Am. Chem. Soc.* **2003**, *125*, 11510-11511. (f) Espino, C. G.; Fiori, K. W.; Kim, M.; Du Bois, J. *J. Am. Chem. Soc.* **2004**, *126*, 15378-15379. (g) Lebel, H.; Huard, K.; Lectard, S. *J. Am. Chem. Soc.* **2005**, *127*, 14198-14199. (h) Kim, M.; Mulcahy, J. V.; Espino, C. G.; Du Bois, J. *Org. Lett.* **2006**, *8*, 1073-1076. (i) Ruppel, J. V.; Kamble, R. M.; Zhang, X. P. *Org. Lett.* **2007**, *9*, 4889-4892. (j) Huard, K.; Lebel, H. *Chem. Eur. J.* **2008**, *14*, 6222-6230. (k) Lu, H.; Tao, J.; Jones, J. E.; Wojtas, L.; Zhang, X. P. *Org. Lett.* **2010**, *12*, 1248-1251. (l) Lu, H.; Jiang, H.; Hu, Y.; Wojtas, L.; Zhang, X. P. *Chem. Sci.* **2011**, *2*, 2361-2366. (m) Nguyen, Q.; Sun, K.; Driver, T. G. *J. Am. Chem. Soc.* **2012**, *134*, 7262-7265.

8. (a) O'Hagen, D. *Nat. Prod. Rep.* **2000**, *17*, 435-446. (b) Pinder, A. R. *Nat. Prod. Rep.* **1984**, *1*, 225-230.
9. (a) Hennessy, E. T.; Betley, T. A. *Science* **2013**, *340*, 591-595. (b) Hennessy, E. T.; Liu, R. Y.; Iovan, D. A.; Duncan, R. A.; Betley, T. A. *J. Am. Chem. Soc.* **2014**, *5*, 1526-1532. (c) Iovan, D. A.; Betley, T. A. *J. Am. Chem. Soc.* **2016**, *138*, 1983-1993.
10. Thacker, N. C.; Lin, Z.; Zhang, T.; Gilhula, J. C.; Abney, C. W.; Lin, W. *J. Am. Chem. Soc.* **2016**, *138*, 3501-3509.
11. Recent reviews on metalloradical catalysis: (a) Clark, A. J. *Eur. J. Org. Chem.* **2016**, 2231-2243. (a) Xue, Z.; He, D.; Xie, X. *Polym. Chem.* **2015**, *6*, 1660-1687. (a) Lyaskovskyy, V.; de Bruin, B. *ACS Catal.* **2012**, *2*, 270-279. (b) Jahn, U. *Top. Curr. Chem.* **2012**, *320*, 191-322.
12. (a) Broere, D. L. J.; de Bruin, B.; Reek, J. N. H.; Lutz, M.; Dechert, S.; van der Vlugt, J. I. *J. Am. Chem. Soc.* **2014**, *136*, 11574-11577. (b) Broere, D. L. J.; van Leest, N. P.; de Bruin, B.; Siegler, M. A.; van der Vlugt, J. I. *Inorg. Chem.* **2016**, *55*, 8603-8611.
13. (a) Bittner, M. M.; Lindeman, S. V.; Popescu, C. V.; Fiedler, A. T. *Inorg. Chem.* **2014**, *53*, 4047-4061. (b) Bittner, M. M.; Lindeman, S. V.; Fiedler, A. T. *J. Am. Chem. Soc.* **2012**, *134*, 5460-5463.
14. (a) Min, K. S.; Weyhermüller, T.; Wieghardt, K. *Dalton Trans.* **2003**, 1126-1132. (b) Sun, X.; Chun, H.; Hildenbrand, K.; Bothe, E.; Weyhermüller, T.; Neese, F.; Wieghardt, K. *Inorg. Chem.* **2002**, *41*, 4295-4303.
15. (a) Broere, D. L. J.; Plessius, R.; van der Vlugt, J. I. *Chem. Soc. Rev.* **2015**, *44*, 6886-6915. (b) Broere, D. L. J.; Metz, L. L.; de Bruin, B.; Reek, J. N. H.; Siegler, M. A.; van der Vlugt, J. I. *Angew. Chem. Int. Ed.* **2015**, *54*, 1516-1520. (c) Broere, D. L. J.; Demeshko, S.; de Bruin, B.; Pidko, E. A.; Reek, J. N. H.; Siegler, M. A.; Lutz, M.; van der Vlugt, J. I. *Chem. Eur. J.* **2015**, *21*, 5879-5886. (d) Broere, D. L. J.; Modder, D. K.; Blokker, E.; Siegler, M. A.; van der Vlugt, J. I. *Angew. Chem. Int. Ed.* **2016**, *55*, 2406-2410. (e) Broere, D. L. J.; Plessius, R.; Tory, J.; Demeshko, S.; de Bruin, B.; Siegler, M. A.; Hartl, F.; van der Vlugt, J. I. *Chem. Eur. J.* **2016**, *22*, 13965-13975. (f) Bagh, B.; Broere, D. L. J.; Siegler, M. A.; van der Vlugt, J. I. *Angew. Chem. Int. Ed.* **2016**, *55*, 8381-8385.
16. Lakshman, T. R.; Chatterjee, S.; Chakraborty, B.; Paine, T. K. *Dalton Trans.* **2016**, *45*, 8835-8844.
17. Gütlich, P. Z. *inorg. allg. Chem.* **2012**, *638*, 15-43.
18. (a) Mukherjee, S.; Weyhermüller, T.; Bill, E.; Wieghardt, K.; Chaudhuri, P. *Inorg. Chem.* **2005**, *44*, 7099-7108. (b) Chun, H.; Bill, E.; Weyhermüller, T.; Wieghardt, K. *Inorg. Chem.* **2003**, *42*, 5612-5620. (c) Chun, H.; Weyhermüller, T.; Bill, E.; Wieghardt, K. *Angew. Chem. Int. Ed.* **2001**, *40*, 2489-2492.
19. (a) Rajput, A.; Sharma, A. K.; Barman, S. K.; Koley, D.; Steinert, M.; Mukherjee, R. *Inorg. Chem.* **2014**, *53*, 36-48. (b) Ali, A.; Barman, S. K.; Mukherjee, R. *Inorg. Chem.* **2015**, *54*, 5182-5194. (c) Ali, A.; Dhar, D.; Barman, S. K.; Lloret, F.; Mukherjee, R. *Inorg. Chem.* **2016**, *55*, 5759-5771.
20. (a) Wong, J. L.; Higgins, R. F.; Bhowmick, I.; Cao, D. X.; Szigethy, G.; Ziller, J. W.; Shores, M. P.; Heyduk, A. F. *Chem. Sci.* **2013**, *4*, 1906-1910. (b) Wong, J. L.; Higgins, R. F.; Bhowmick, I.; Cao, D. X.; Szigethy, G.; Ziller, J. W.; Shores, M. P.; Heyduk, A. F. *Chem. Sci.* **2016**, *7*, 1594-1599.
21. (a) Brown, S. N. *Inorg. Chem.* **2012**, *51*, 1251-1260. See also: (b) Bhattacharya, S.; Gupta, P.; Basuli, F.; Pierpont, C. G. *Inorg. Chem.* **2002**, *41*, 5810-5816.
22. Löwdin, P. *J. Chem. Phys.* **1950**, *18*, 365-375.
23. (a) Blanksby, S. J.; Ellison, G. B. *Acc. Chem. Res.* **2003**, *36*, 255-263. (b) For substrates **S₇**-**S₉**, the substrate with the weaker C-H bond is more easily converted. The bond dissociation energy (BDE) at 298 K (ΔH_{298}) of the benzylic C-H bond in toluene is 89.8 kcal mol⁻¹. The BDE (ΔH_{298}) of benzylic C-H bond of ethylbenzene (77.6 kcal mol⁻¹) is ca. 12 kcal mol⁻¹ lower than that of toluene. Therefore, C-H bond activation of **S₇** (o-substituted ethylbenzene) is easier than **S₈** and **S₉** (o-substituted toluene) and this is reflected in higher yield of **P_{7a}** (53%) compared to **P_{8a}** (46%) or **P_{9a}** (44%). Substrates **S₂** and **S₁₀** with similar allylic C-H bonds gave similar yields of products (**P_{2a}** 96%, **P_{10a}** 95%). The BDEs (ΔH_{298}) of allylic C-H bonds are very similar to those of benzylic C-H bonds: propene (88.8 kcal mol⁻¹) vs. toluene (89.8 kcal mol⁻¹), 1-butene (76.5 kcal mol⁻¹) vs. ethylbenzene (77.6 kcal mol⁻¹), 1-pentene (75.4 kcal mol⁻¹) vs. n-propylbenzene (76.4 kcal mol⁻¹). However, **S₂** with an allylic C-H bond gave **P_{2a}** in high yield (96%), while **S₁** with a benzylic C-H bond resulted in only 65% of **P_{1a}**. The BDE (ΔH_{298}) of a benzylic C-H bond adjacent to an alkoxy group is comparable to the BDE (ΔH_{298}) of a benzylic C-H bond adjacent to an alkyl group. However, **S₆** gave 92 % of **P_{6a}**, whereas **S₁** gave only 65 % of **P_{1a}**. So, no clear correlation between C-H bond strength of substrates and yields of products can be found for **S₁**, **S₂** and **S₆**.
24. Sharon, D. A.; Mallick, D.; Wang, B.; Shaik, S. *J. Am. Chem. Soc.* **2016**, *138*, 9597-9610.
25. ICP-AAS analysis confirmed <10 ppm levels for Co, Rh, Ir, Ni, Pd and Cu, see SI for details.
26. a) Korstanje, T. K.; van der Vlugt, J. I.; Elsevier, C. J.; de Bruin, B. *Science* **2015**, *350*, 298-302. b) Drost, R. M.; Rosar, V.; Dalla Marta, S.; Lutz, M.; Demitri, N.; Milani, B.; de Bruin, B. Elsevier, C. J. *ChemCatChem* **2015**, *7*, 2095-2107.
27. Review on nitrogen-centered ligand radicals: Olivos Suarez, A.I.; Lyaskovskyy, V.; Reek, J.N.H.; van der Vlugt, J.I.; de Bruin, B. *Angew. Chem. Int. Ed.* **2013**, *52*, 12510-12529.
28. Experimental detection of cobalt nitrene radical species: (a) Goswami, M.; Lyaskovskyy, V.; Domingos, S. R.; Buma, W. J.; Woutersen, S.; Troeppner, O.; Ivanović-Burmazović, I.; Lu, H.; Cui, X.; Zhang, X. P.; Reijerse, E. J.; DeBeer, S.; van Schooneveld, M. M.; Pfaff, F. F.; Ray, K.; de Bruin, B. *J. Am. Chem. Soc.* **2015**, *137*, 5468-5479. (b) Lyaskovskyy, V.; Olivos Suárez, A. I.; Lu, H.; Jiang, H.; Zhang, X. P.; de Bruin, B. *J. Am. Chem. Soc.* **2011**, *133*, 12264-12273.
29. Stoichiometric reactions between complex **1** and Boc₂O, resulted in full recovery of **1**. This suggests that the catalyst activation process by Boc₂O is most likely an energetically uphill process generating the active form of the catalyst as a short-lived species in rather low concentrations.
30. Slow diffusion of pentane into the blue-green solution led to almost quantitative precipitation of microcrystalline blue solid but attempts to analyze this species by single crystal X-ray structure determination were unsuccessful to date.
31. The C(sp³)-H amination of **S₁** in the presence of Boc₂O with **1** and TIPF₆ (both 5 mol%) led to the formation of **P_{1a}** and **P_{1b}** in the same ratio of ~1.6:1 as observed under the standard conditions.

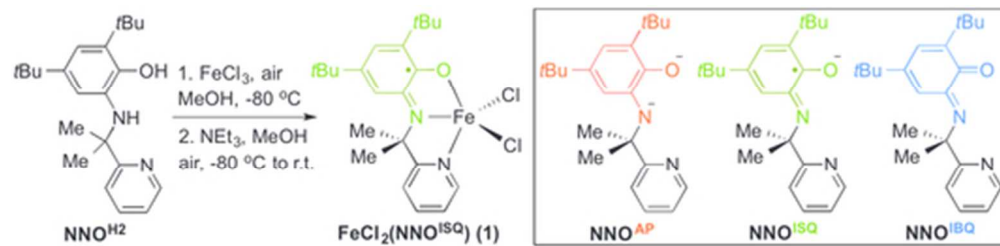




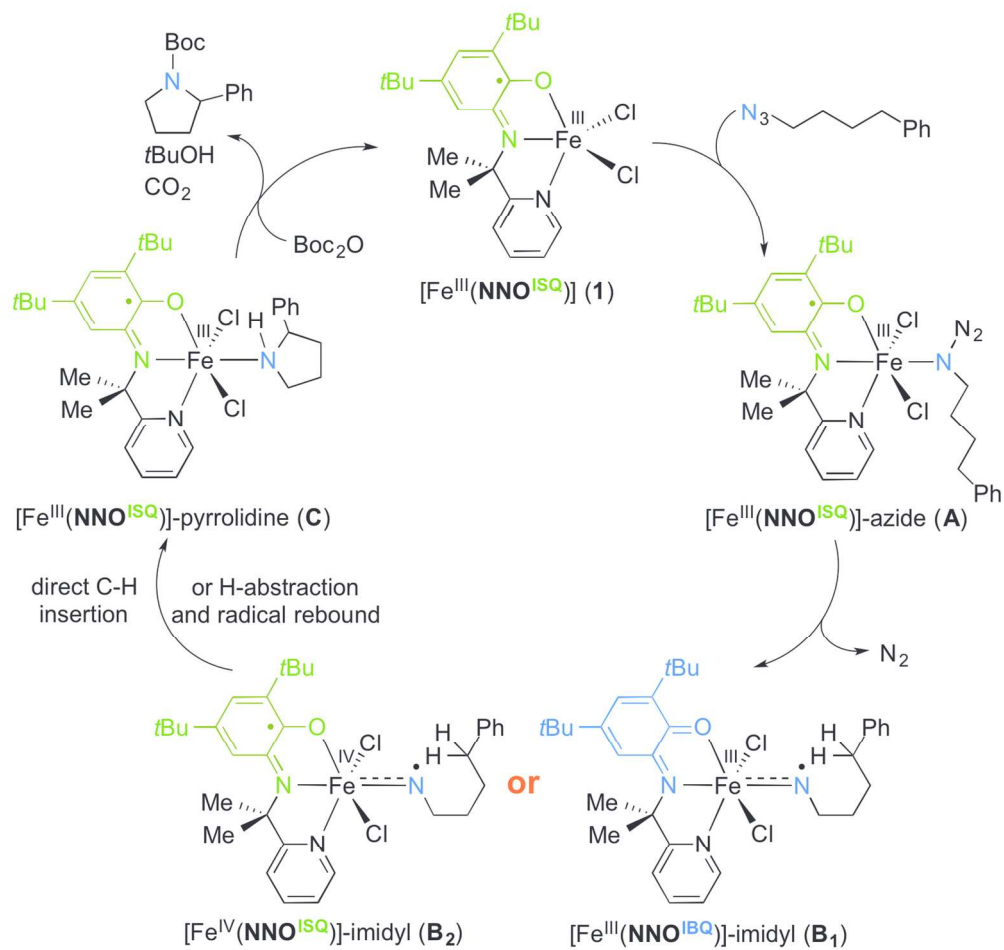
131x21mm (300 x 300 DPI)



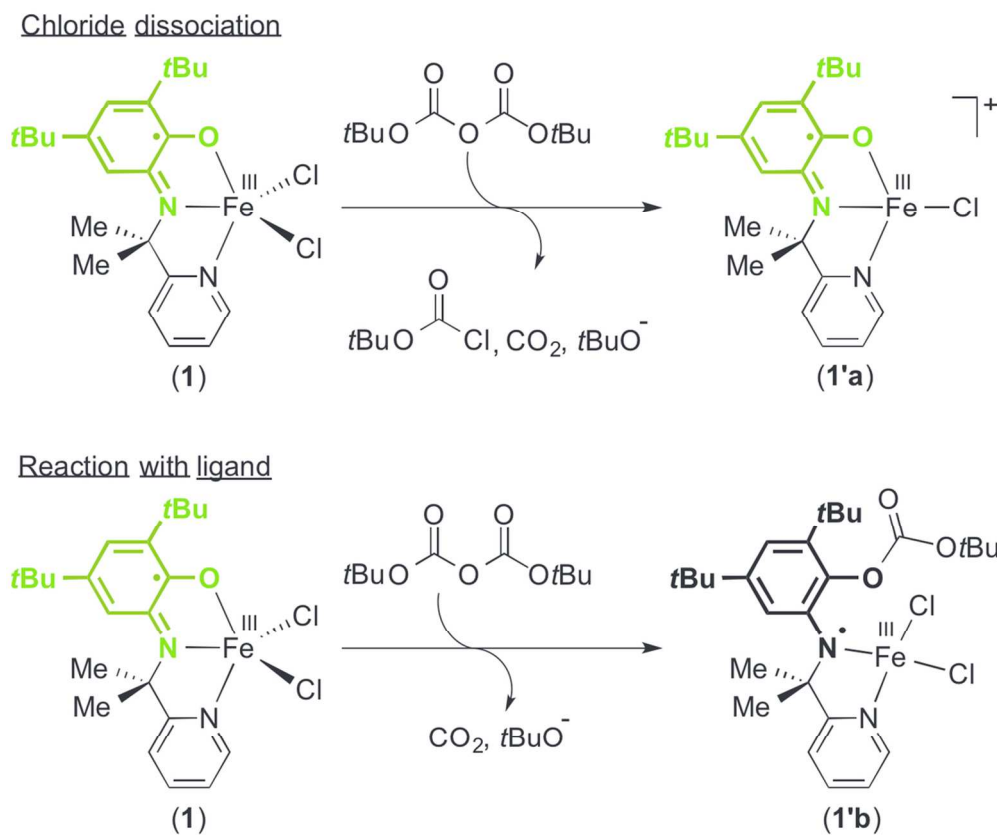
165x217mm (300 x 300 DPI)



45x11mm (300 x 300 DPI)

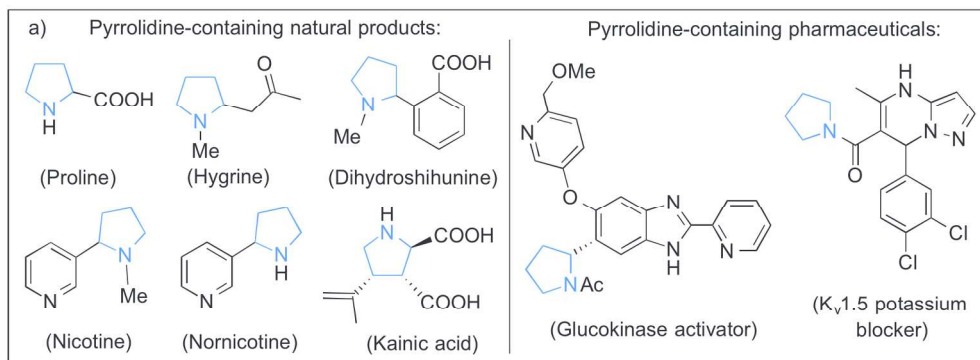


140x133mm (300 x 300 DPI)

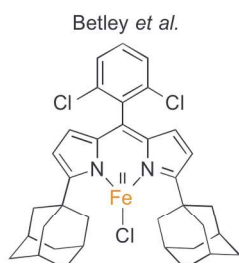
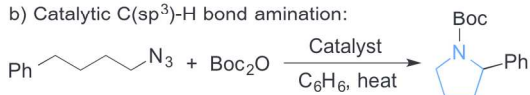


this is Scheme 5 in the revised version as submitted

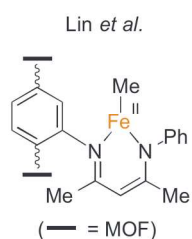
105x87mm (300 x 300 DPI)



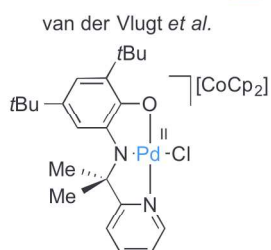
b) Catalytic C(sp³)-H bond amination:



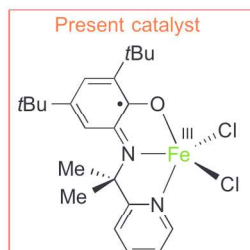
Reaction conditions:
 Boc₂O (1 eq.), 65 °C, 12 h
 Catalyst (10 mol%)
 Yield: 57 %, TON ~ 6



Reaction conditions:
 Boc₂O (10 eq.), 90 °C
 Yield: 90 %, TON ~ 18
 (Homogeneous system:
 Yield: 31 %, TON ~ 6)

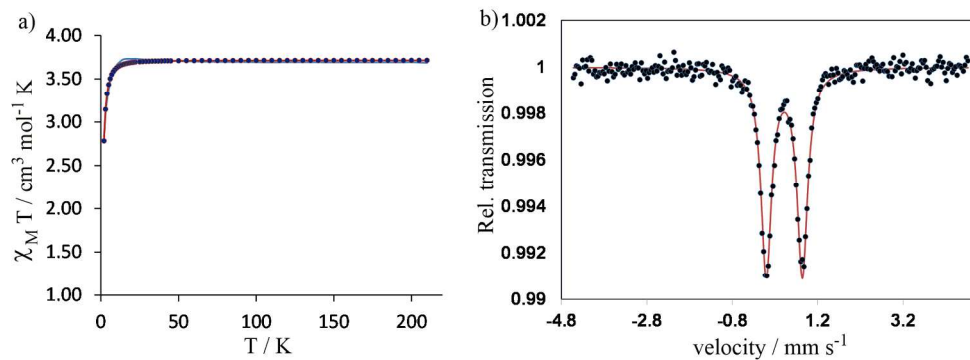


Reaction conditions:
 Boc₂O (1 eq.), 100 °C, 24 h
 Catalyst (10 mol%)
 Yield: 10 %, TON ~ 1

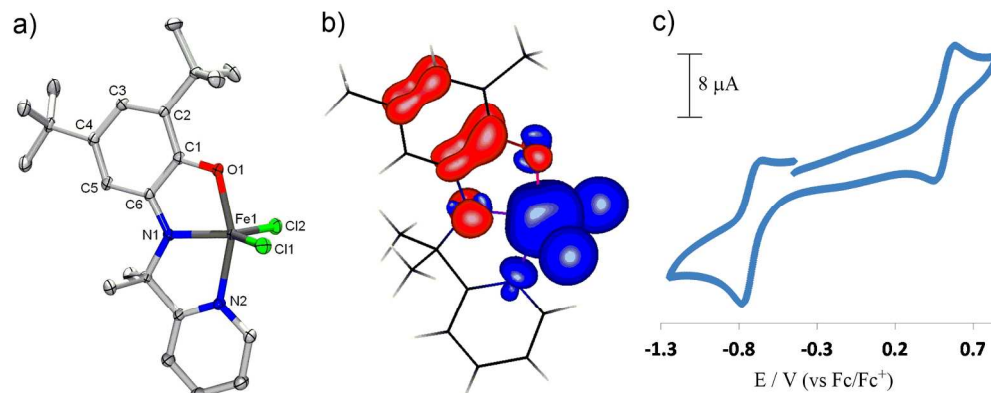


Reaction conditions:
 Boc₂O (1 eq.), 100 °C, 12 h
 Catalyst (1 mol%)
 Yield: 62 %, TON ~ 62

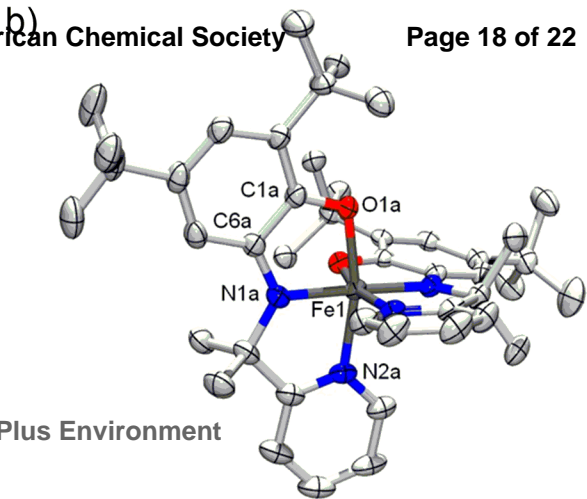
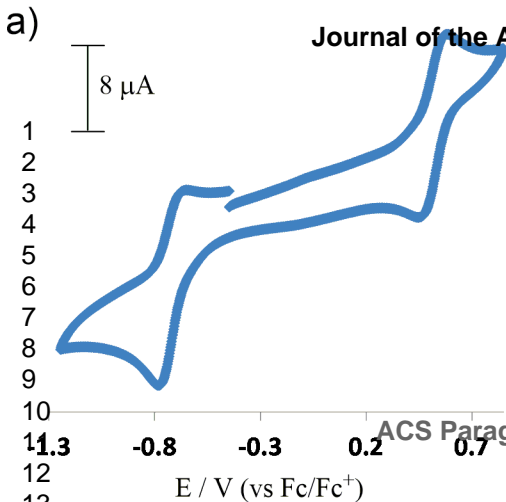
174x158mm (300 x 300 DPI)

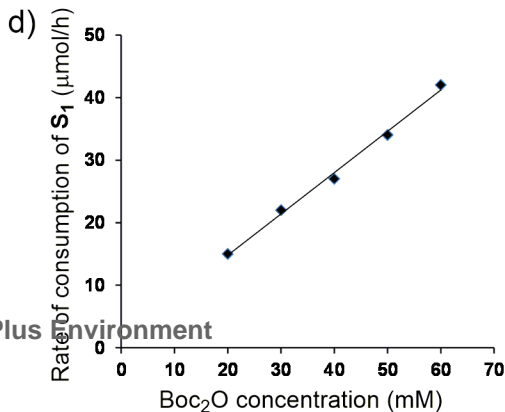
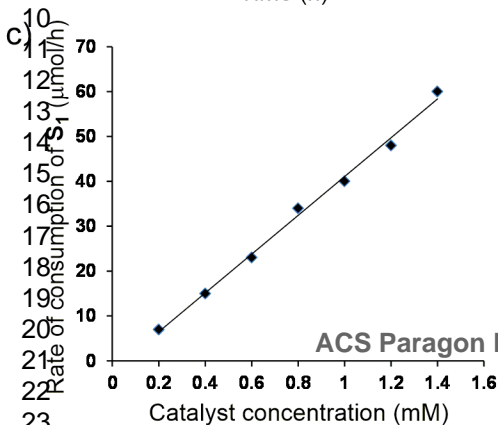
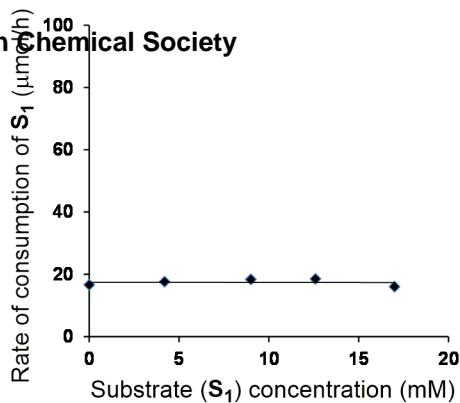
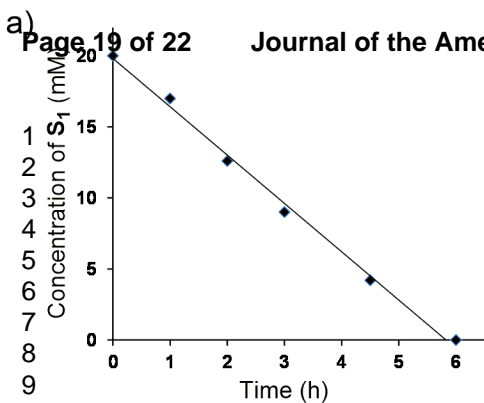


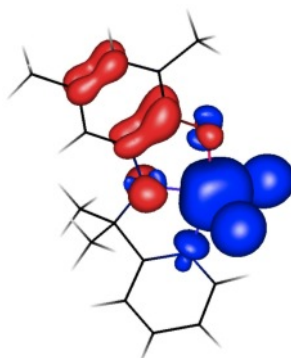
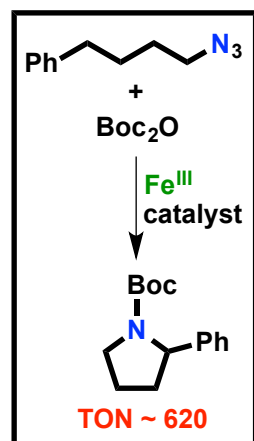
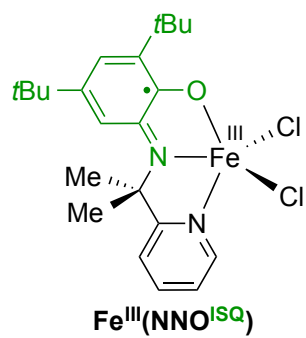
186x67mm (300 x 300 DPI)

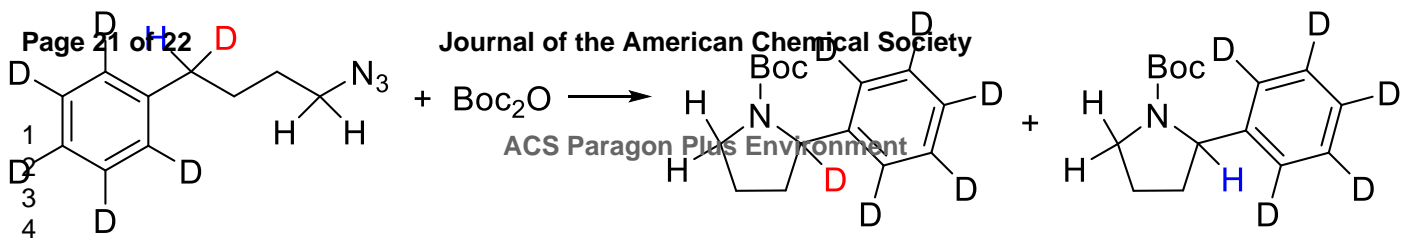


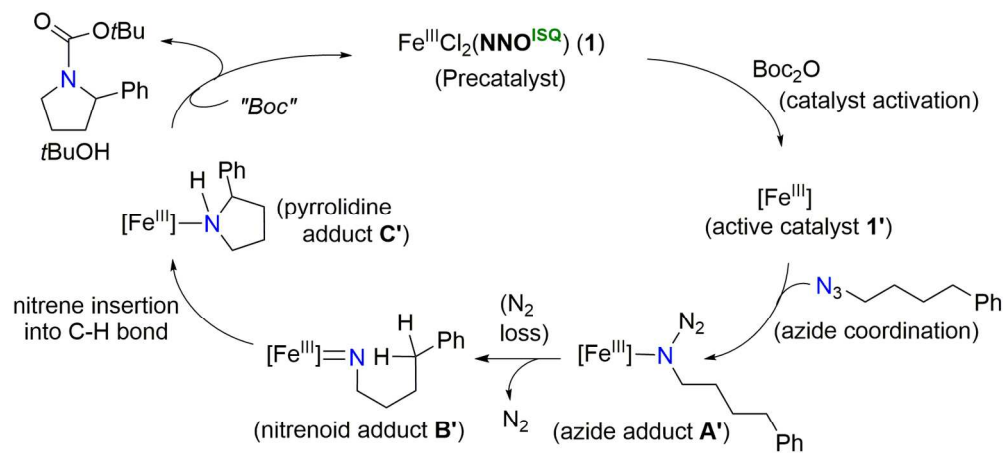
179x73mm (300 x 300 DPI)



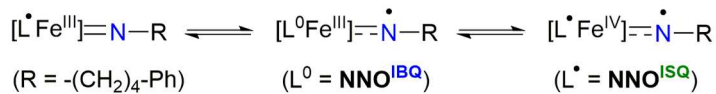








Possible electronic structures of nitrenoid adduct:



150x94mm (300 x 300 DPI)

1
2
3
4
5
6
7
8
9
10
11
12
13
14
15
16
17
18
19
20
21
22
23
24
25
26
27
28
29
30
31
32
33
34
35
36
37
38
39
40
41
42
43
44
45
46
47
48
49
50
51
52
53
54
55
56
57
58
59
60